The Astrophysical Journal Letters, 887:L12 (7pp), 2019 December 10 https://doi.org/10.3847/2041-8213/ab58d1

Exploring the Outskirts of Globular Clusters: The Peculiar Kinematics of NGC 3201

P. Bianchini, R. Ibata, and B. Famaey
Observatoire Astronomique de Strasbourg, Université de Strasbourg, CNRS UMR7550, F-67000 Strasbourg, France; paolo.bianchini@astro.unistra.fr
Received 2019 September 6; revised 2019 November 15; accepted 2019 November 19; published 2019 December 6

Abstract

The outskirts of globular clusters (GCs) simultaneously retain crucial information about their formation mechanism and the properties of their host galaxy. Thanks to the advent of precision astrometry both their morphological and kinematic properties are now accessible. Here we present the first dynamical study of the outskirts of the retrograde GC NGC 3201 until twice its Jacobi radius (<100 pc), using specifically selected high-quality astrometric data from *Gaia* DR2. We report the discovery of a stellar overdensity along the southeast/northwest direction that we identify as tidal tails. The GC is characterized globally by radial anisotropy and a hint of isotropy in the outer parts, with an excess of tangential orbits around the lobes corresponding to the tidal tails, in qualitative agreement with an *N*-body simulation. Moreover, we measure flat velocity dispersion profiles, reaching values of 3.5 ± 0.9 km s^{-1} until beyond the Jacobi radius. While tidal tails could contribute to such a flattening, this high velocity dispersion value is in disagreement with the expectation from the sole presence of potential escapers. To explain this puzzling observation, we discuss the possibility of an accreted origin of the GC, the presence of a dark matter halo—leftover of its formation at high redshift—and the possible effects of non-Newtonian dynamics. Our study uncovers a new path for the study of GC formation and of the properties of the Milky Way potential in the era of precision astrometry.

Unified Astronomy Thesaurus concepts: Globular star clusters (656); Proper motions (1295); Stellar dynamics (1596); Milky Way Galaxy (1054); Tidal tails (1701); Dynamical evolution (421)

1. Introduction

The origin of globular clusters (GCs) is one of the open questions in modern astrophysics. Numerous pieces of evidence indicate that some of the Milky Way (MW) GCs formed in accreted dwarf galaxies (e.g., Leaman et al. 2013; Massari et al. 2019); yet, it is still unclear whether they originated in the early universe within dark matter mini-halos or simply as gravitationally bound clouds (e.g., Peebles 1984; Peñarrubia et al. 2017).

Important clues on the origin of GCs come from the study of their current properties. Despite the fact that their structure is strongly shaped by their >10 Gyr long internal processes (relaxation processes and stellar evolution) and by the gravitational interaction with their host galaxy, primordial long-lasting features imprinted at formation can survive. In particular, the outskirts of GCs, characterized by long relaxation times, are the unique environment to hunt for these primordial properties. Moreover, they represent the test bed to study the transition between internally driven dynamical processes (e.g., internal relaxation, evaporation) and external processes driven by the host galaxy (e.g., tidal stripping, formation of tidal tails). Therefore, the study of the outskirts of GCs offers important clues on their long-term evolution as well as on the properties of the MW potential.

Observationally, a number of studies have shown that the outskirts of some GCs are characterized by extended stellar structures and tidal debris beyond their nominal tidal radius (Grillmair et al. 1995; Leon et al. 2000; Chun et al. 2010; Kuzma et al. 2018). Kinematically, a few line-of-sight velocity studies have indicated that some GCs exhibit flattened velocity dispersion profiles (Drukier et al. 1998; Scarpa et al. 2007; Lane et al. 2010; Da Costa 2012; Bellazzini et al. 2015). Different—but yet not conclusive—explanations for these phenomena have been put forward: (i) the presence of energetically unbound stars still orbiting within the GCs (potential stellar escapers; Fukushige & Heggie 2000; Küpper et al. 2010); (ii) the presence of dark matter, relic of a primordial subhalo in which GCs formed (e.g., Ibata et al. 2013); (iii) modified Newtonian dynamics (e.g., Hernandez et al. 2013). A full morphological and dynamical characterization of the outer regions of GCs is therefore still needed to disentangle these scenarios.

With the recent advances in the field of precision astrometry led by *Gaia* DR2 (Gaia Collaboration et al. 2018a, 2018b), the study of *both the kinematic and morphological properties* of (virtually all) MW GCs up to their outer regions is now possible (see, e.g., Bianchini et al. 2018a). In this Letter, we report the first dynamical study of a GC, NGC 3201, from its intermediate regions until beyond its Jacobi radius ($\lesssim$100 pc) using *Gaia* DR2 proper motions. In this work, we will refer to the tidal truncation radius r_t as an approximation of the boundary of the GC obtained from fitting its surface brightness profile. The actual physical border of the cluster is identified by the Jacobi radius, r_j, that is the distance between the first Lagrangian point and the center of the cluster, roughly representing the boundary radius inside of which the cluster is gravitationally dominant with respect to the Galaxy.

NGC 3201, at a distance of 4.9 kpc (Harris 1996), is characterized by a retrograde and eccentric orbit (Gaia Collaboration et al. 2018b), an intermediate relaxation time ($\log T_{\rm rel}$ yr$^{-1} = 9.27$, Zocchi et al. 2012) suggesting a not very efficient internal dynamical evolution, and the presence of a few extra-tidal stars (Kunder et al. 2014; Anguiano et al. 2016; Kundu et al. 2019). We initially spotted the presence of the tidal tail around NGC 3201 by searching close to the Galactic plane with the `STREAMFINDER` algorithm (Malhan & Ibata 2018), and noticed that it appears to link up with the Gjöll stream (Ibata et al. 2019). These new stream maps will be presented in a forthcoming contribution (R. Ibata et al. 2019, in

Table 1
Structural and Orbital Properties of NGC 3201

$d_\odot$ (kpc)	d_{GC} (kpc)	Pericenter (kpc)	Apocenter (kpc)	M ($M_\odot$)	$\log T_{rel}$ (yr)	r_h (pc)	r_h (arcmin)	r_t (pc)	r_t (arcmin)	r_j (pc)	r_j (arcmin)
4.9 (1)	8.8 (1)	8.5 (2)	22–29 (2)	3.98×10^5 (3)	9.27 (1)	4.41 (1)	3.10	36.11 (1)	25.35	83.46 (4)	58.58

Note. Distance to the Sun $d_\odot$, distance to the galactic center d_{GC}, pericenter and apocenter, total mass M from the Wilson model fit, half-light relaxation time T_{rel}, half-light radius r_h, tidal truncation radius r_t, Jacobi radius r_j. (1) Harris (1996), (2) Gaia Collaboration et al. (2018b), (3) McLaughlin & van der Marel (2005), (4) Balbinot & Gieles (2018).

preparation). These properties (reported in Table 1) make NGC 3201 an ideal target to pioneer studies on the external regions of GCs and to unveil their formation and evolution.

2. Cluster Member Selection

To probe the dynamics of the outer regions of a GC we need to select high-quality proper motion measurements suitable for a kinematic analysis, and, at the same time, minimize background and foreground contaminations from likely non-cluster members. As a first step, we consider the member stars used in Gaia Collaboration et al. (2018b) and perform a series of quality cuts to select high-precision astrometric data and avoid measurements affected by crowding. These cuts, based on parameters provided in the *Gaia* DR2 catalog and following the procedures illustrated in Lindegren et al. (2018) (see also Vasiliev 2019; Jindal et al. 2019) include:

1. `astrometric_gof_al` < 0.5;
2. `astrometric_excess_noise` < 1;
3. `phot_bp_rp_excess_factor` $< 1.3 + 0.06(\mathrm{bp-rp})^2$;
4. `ruwe` $<$ `ruwe`$_{95}$, that is the 95th percentile of the renormalized unit weight error, `ruwe` (see https://www.cosmos.esa.int/web/gaia/dr2-known-issues for a definition).

This brings the sample from a total of 19,922 to 8222 stars within the Jacobi radius of the cluster ($r_j = 83.46$ pc/58.′58; Balbinot & Gieles 2018). To extend the sample beyond the Jacobi radius of the cluster we select an outer sample of stars within $10\,r_h < r < 2\,r_j$, with $r_h = 3.'10$, half-light radius of the cluster (Harris 1996), allowing an overlap with the inner sample. We apply the same high-quality proper motion criteria employed above and select the member stars based on proper motions, $G_{rp} - G_{bp}$ color, G magnitude, and parallax, using `TOPCAT`. This step is visualized in Figure 1. The stars, in (R.A., decl.) and ($\mu_{\mathrm{R.A.}}$, $\mu_{\mathrm{decl.}}$), are projected into a Cartesian coordinate system (x, y) and (μ_x, μ_y) using Equation (2) of Gaia Collaboration et al. (2018b), with positive x- and μ_x-axes pointing west. We subtract from the velocities the mean motion of NGC 3201, $(\mu_x, \mu_y) = (-8.3344, -1.9895)$ mas yr^{-1}.

First, stars from the outer sample are selected to match the color–magnitude properties of the inner sample and the parallax versus G magnitude diagram. Subsequently, only stars within 1 mas yr^{-1} of the μ_x–μ_y diagram are considered, giving a sample of 8271 stars. We also consider a looser cut in the velocity space that includes all stars within 2 mas yr^{-1} (see Section 3). A clear overdensity is visible along the southeast/northwest direction in the field of view (FoV) of the cluster (top left panel of Figure 1), indicating the discovery of tidal tail structures around NGC 3201. This observed feature is independent of the cut adopted in the velocity space.

Since field contamination can be very critical in the outer part of the cluster, we follow a decontamination technique similar to the one outlined in Carballo-Bello (2019). We select a field sample ranging from $2\,r_j < r < 2.5\,r_j$ and apply the same quality cuts as the ones applied to the members. For a given four-dimensional bin of magnitude, color, μ_x, and μ_y, we calculate the surface number density of field stars and cluster stars n_{field} and n_{cluster} and we associate to each star a contamination factor $w = 1 - n_{\mathrm{field}}/n_{\mathrm{cluster}}$. We consider magnitude cells of 0.5 mag, color cells of 3 mag, and velocity cells of 2 mas yr^{-1}, in the intervals $8 < G < 21$ mag, $-1 < G_{rp} - G_{bp} < 4$ mag, and $-4 < \mu < 4$ mas yr^{-1}. We further recalculate w after shifting the starting position in steps of 1/10, 1/5, and 1/10, in magnitude, color, and velocity, respectively, in order to minimize the low-number statistical fluctuation due to the bin selection.

Globally, our analysis shows that the contamination level expected in our sample is ∼13%; this indicates that in the outskirts of the cluster, prior to decontamination, only approximately ∼13 stars (out of the 102 stars with radius $R > 50'$) are expected to be contaminants. For each star we compute the average contamination factor w and we exclude from our sample those stars with $w < 0.9$. A total of 33 stars are discarded, further indicating a low contamination from field stars.[1] Our final clean sample consists of 8238 NGC 3201 member stars with high-quality proper motion measurements, extending from $\sim r_h$ beyond r_j and include the tidal tail structure discovered here.

3. Kinematic Analysis

We decompose the proper motions into radial and tangential components (μ_r, μ_t) and we propagate the velocity uncertainties and the covariances. The kinematic profiles (mean proper motion profiles, velocity dispersion profiles, and anisotropy profile) are computed using the likelihood function presented in Bianchini et al. (2018a, see their Equations (2) and (3)) with the addition of the covariance term (see, e.g., Sollima et al. 2019, Equation (3)). The sample is divided in annular bins and for each bin the likelihood is sampled using the Markov Chain Monte Carlo algorithm `emcee` by Foreman-Mackey et al. (2013).

A biased assessment of the proper motions errors can have a high impact on the velocity dispersion measurements, particularly in the outskirts of the cluster where dispersions are expected to be low. We minimized this problem by selecting only high-quality astrometric measurements. Moreover, as shown in Gaia Collaboration et al. (2018a), *Gaia* DR2 proper

[1] We checked different values of the contamination threshold, and the final results are not affected by this choice.

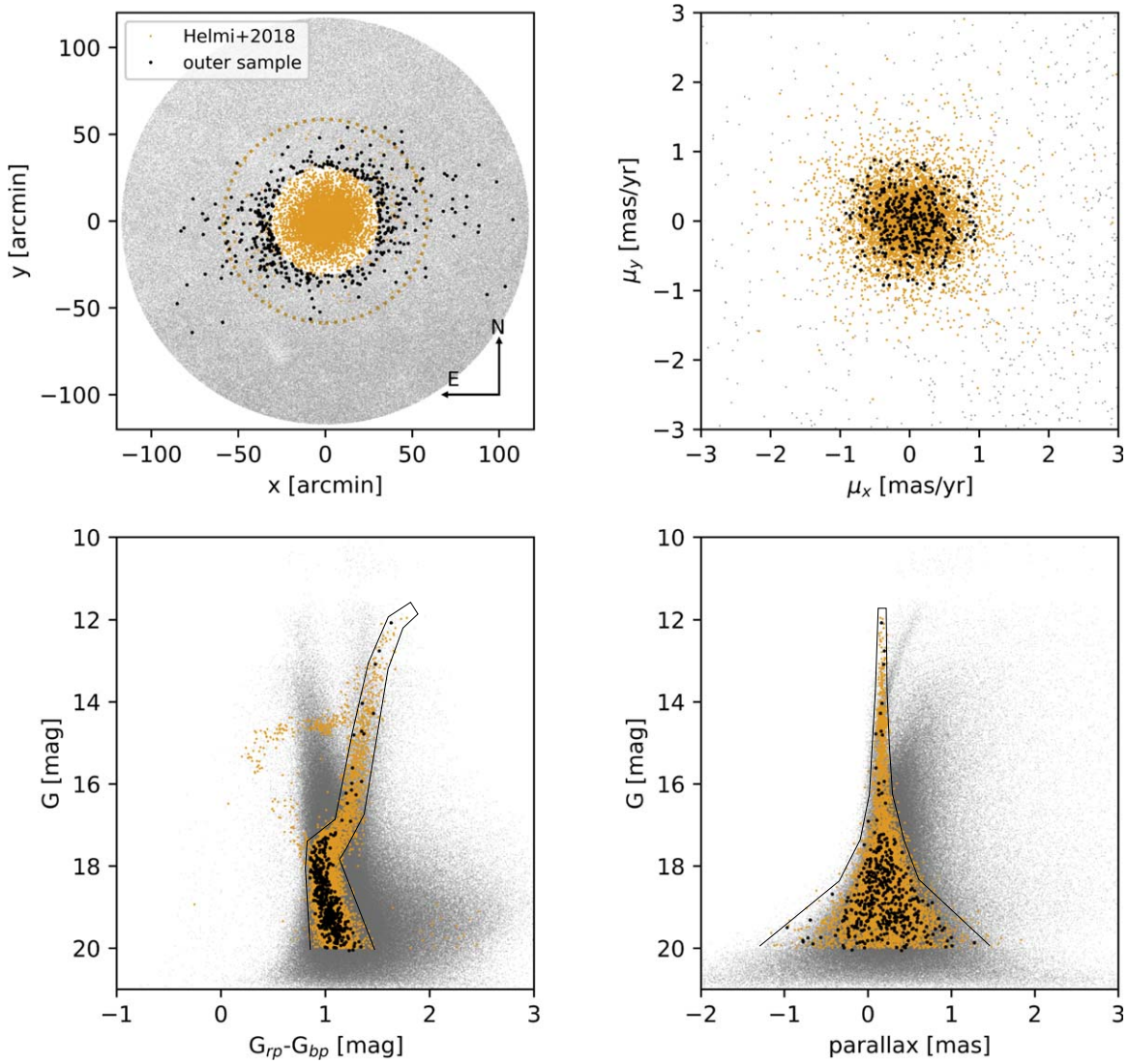

Figure 1. NGC 3201 member star selection in the area extending to 2 r_j. The orange points are the inner sample member stars from Gaia Collaboration et al. (2018b), the gray points all the stars in the 2 r_j FoV, and the black dots are the outer stars selected as members in this Letter. The membership selection is based on the properties of the μ_x–μ_y diagram (top right panel), color–magnitude diagram (bottom left panel), and the parallax vs. G magnitude diagram (bottom right panel) of the inner sample. Only high-quality proper motion measurements suitable for dynamical analysis are included in the sample. Top left: the FoV of NGC 3201 clearly shows the presence of tidal tail structures in the outskirts of the cluster, extending beyond the Jacobi radius (dashed line).

motion errors are underestimated by a factor of ∼10% for stars with magnitude $G > 16$ and of ∼30% for stars with $G < 13$. We include this additional correction before performing the kinematic measurements.

Finally, we test the presence of magnitude-dependent biases. For this purpose, we calculate the kinematic profiles for stars in magnitude bins (red giant branch $G < 17$, $17 < G < 18$, $18 < G < 19$, $G > 19$). We find that all the profiles are consistent with each other, indicating that any magnitude-dependent systematics are within the error uncertainties. Note that the range of magnitude covered corresponds to a stellar mass range of $\sim 0.6 - 0.8\ M_{\odot}$[2]; therefore, the lack of differences in velocity dispersion also indicates that the system, at least in the outer part $> r_h$, is far from a state of partial energy equipartition. This is fully consistent with the theoretical expectation for the outer areas of GCs where two-body relaxation processes are expected to be less efficient in shaping the internal dynamics (Trenti & van der Marel 2013; Bianchini et al. 2016, 2018b).

In Figure 2 we show the velocity dispersion profiles σ_r and σ_t and the anisotropy profile calculated as the ratio of the two. In order to increase the spatial resolution around the outskirts of the GC we employed the following binning: within the tidal radius (gray circles, $r_t = 25\farcm35$; Harris 1996) each bin contains 823 stars; for the outer region (black circles) each bin contains 195 stars.

The inner parts of the velocity dispersion profiles are consistent with line-of-sight velocity measurements (Baumgardt & Hilker 2018; see the red line in Figure 2), while the outer parts, measured here for the first time, show a flattening around the Jacobi radius to values $\sim 0.1 - 0.2$ mas yr^{-1} ($\sim$2.5–4 km s^{-1}). We calculate a velocity dispersion at the Jacobi radius of $\sigma_r = 0.14 \pm 0.04$ mas yr^{-1} and $\sigma_t = 0.16 \pm 0.04$ mas yr^{-1} (with an average over the two components of 3.5 ± 0.9 km s^{-1}), defined as the velocity dispersion at $R > 50'$, comprising 102 stars. The last point in

[2] Stellar masses from PARSEC isochrones (Marigo et al. 2017).

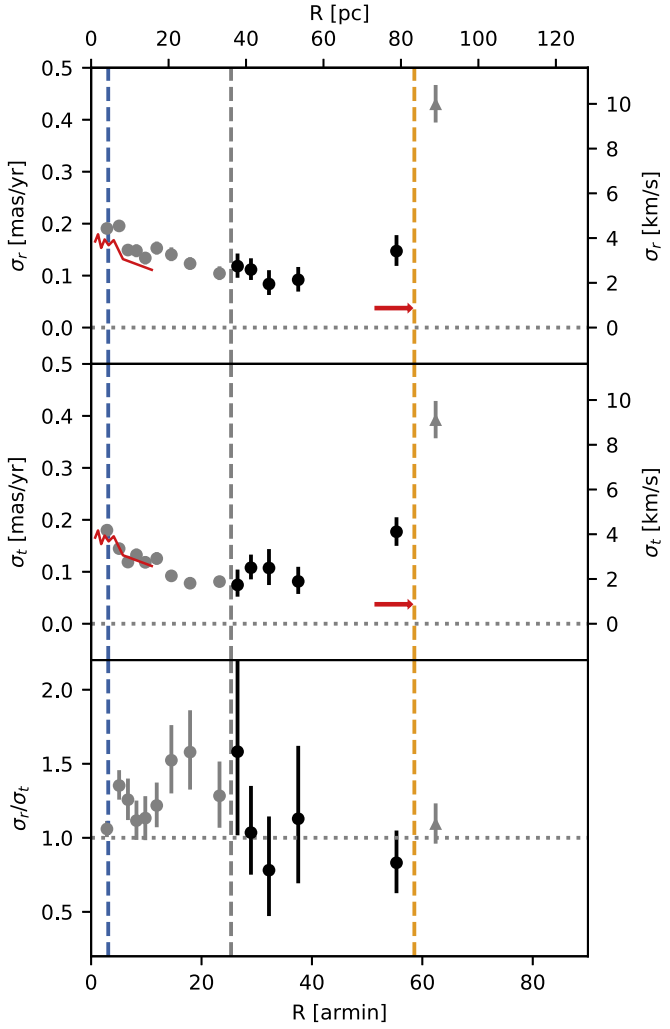

Figure 2. From top to bottom: velocity dispersion profiles for the radial and tangential component of the proper motions σ_r and σ_t, and velocity anisotropy profile. Gray circles refer to the region within the tidal radius, while the black circles refer to the outskirts of the cluster; the gray triangles correspond to the values obtained from a looser proper motion cut (see Section 2). The dashed lines are the half-light radius, tidal radius, and Jacobi radius, in blue, gray, and orange, respectively. The red line is the line-of-sight velocity dispersion profile from Baumgardt & Hilker (2018). The velocity dispersion profiles show an evident flattening in the outskirts and higher values than what is expected from the presence of potential escapers only (red arrow; Claydon et al. 2017). NGC 3201 is radially anisotropic in the intermediate regions and isotropic in the outskirts.

each panel is derived using the looser selection cut in the velocity–velocity space (see Section 2) and presents a high value of velocity dispersion ($0.5\,\mathrm{mas\,yr^{-1}}/11\,\mathrm{km\,s^{-1}}$) that very likely indicates a stronger field contamination or the presence of unbound stars. We discuss the implication of the flattening of the velocity dispersion profiles in Section 4.

The bottom panel of Figure 2 shows that NGC 3201 is characterized by radial anisotropy in the intermediate region, with a hint for a radial variation toward isotropy in the outskirts (although only marginally significant, also given the additional error systematics in *Gaia* DR2 of the order of $\sim$0.07 mas yr^{-1}; Lindegren et al. 2018). Globally, the cluster is characterized by a clear signature of radial anisotropy $\sigma_r/\sigma_t = 1.25 \pm 0.04$ that can be taken as the result of internal relaxation processes, consistent with its intermediate relaxation condition (Zocchi et al. 2012). The trend of the anisotropy profile is in agreement with what found by Jindal et al. (2019) for a sample of MW GCs and suggests an isotropization in the outskirts due to the effect of the Galactic tidal field that progressively strips stars on radial orbit (e.g., Baumgardt & Makino 2003; Sollima et al. 2015; Tiongco et al. 2016; Zocchi et al. 2016; Bianchini et al. 2017; see also Figure 4 in Section 3.1).

Finally, we note that the mean velocity profiles are consistent with the prediction obtained in Bianchini et al. (2018a): the radial component shows a perspective contraction due to the receding motion of the GC (Equation (4) of van de Ven et al. 2006; Bianchini et al. 2018a) and the tangential component shows no significant sign of rotation within $0.05\,\mathrm{mas\,yr^{-1}}/1\,\mathrm{km\,s^{-1}}$. This result assures that data systematics are under control below the $\sim$1 km s^{-1} level.

3.1. Comparison with a Dynamical Simulation

To understand the qualitative effects of tidal tails on GC kinematics, we analyze an *N*-body simulation that exhibits tidal tails in the final snapshot. The simulation was reported as DWL-MW10-evap in Bianchini et al. (2017) and Miholics et al. (2016) and consists of $N = 50{,}000$ initial particles evolved for 10 Gyr in a time-dependent tidal field. The simulation was run with `NBODY6TT` (Renaud & Gieles 2015) and includes a stellar mass function and stellar evolution.

In Figure 3, we show one projection of the simulation and the velocity dispersion profiles along the radial and tangential components of the proper motions and along the line of sight. The dispersion profiles show a behavior qualitatively similar to the one we observed for NGC 3201, indicating that tidal tails can contribute to the flattening of the velocity dispersion in the outskirts of the GC. Note, however, that in our observation the value of velocity dispersion at the Jacobi radius is similar to the one at the half-light radius, while for the simulation this is a factor $\sim$2 lower. This suggests that additional processes are contributing to the observed flattening of NGC 3201 (see Section 4); properly tailored simulations to NGC 3201 are still needed for a conclusive comparison with data.

Furthermore, we compute the velocity dispersion maps, dividing the FoV in equal number spatial bins ($\approx$300 stars per bin), using the Voronoi binning algorithm (Cappellari & Copin 2003). Figure 4 shows the comparison between the simulated and observed maps. Both observation and simulation show a tangential velocity dispersion that is higher along the major axis of the system, connecting the points where the tidal tails begin. In contrast, the radial component of the velocity dispersion exhibits a feature that is perpendicular to that of the tangential component. These differences in the spatial distribution of velocity dispersions can be explained by the progressive stripping of stars on radial orbits by the Galactic tidal field that will escape through the Lagrangian points and form the tidal tails. As a result, an excess of stars in tangential orbits are left around the Lagrangian points. This excess of tangential orbits allows us to identify the approximate location of the Lagrangian points, lying along the northwest/southeast direction.

4. Flattening of the Velocity Dispersion Profiles

The dynamics of the outskirts of GCs is known to be characterized by the presence of potential escapers, which are stars that are energetically unbound but still orbiting within the GC (e.g., Fukushige & Heggie 2000; Küpper et al. 2010;

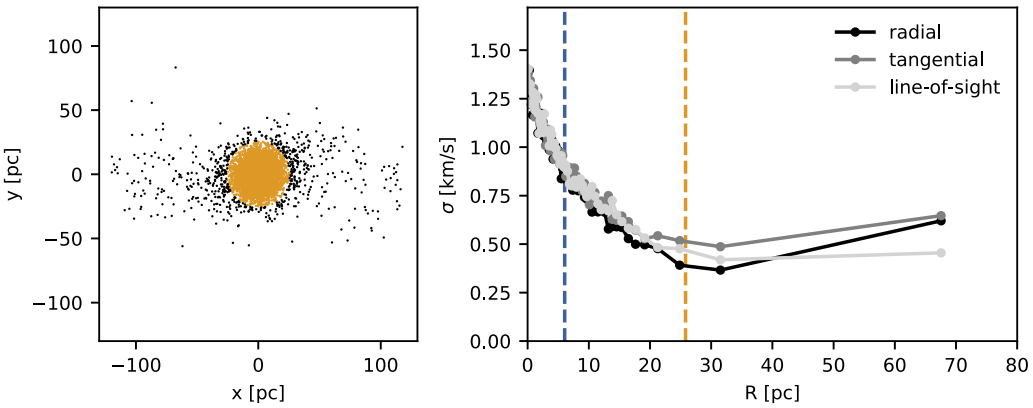

Figure 3. Projected view of a snapshot at 10 Gyr of an *N*-body simulation forming tidal tails (see Miholics et al. 2016; Bianchini et al. 2017). Orange points indicate stars inside the cluster's Jacobi radius. The right panel shows that the velocity dispersion profiles of the three velocity components flatten at radii larger than the Jacobi radius (orange dashed line). The blue dashed line is the half-light radius.

Daniel et al. 2017). The number of potential escapers is comparable to the number of bound stars around $0.5\,r_j$ and dominates at larger radii (Claydon et al. 2017). As a result, they produce a flattening of the velocity dispersion profile. Claydon et al. (2017) provide a theoretical expectation of the velocity dispersion at the Jacobi surface given the GC mass, orbit, and the mass profile of the host galaxy. For NGC 3201 this value is $0.87\,\mathrm{km\,s^{-1}}$ as indicated in Figure 2 with a red arrow. It is evident that our velocity dispersion measurement at the Jacobi radius $3.5 \pm 0.9\,\mathrm{km\,s^{-1}}$ is $\sim 3\sigma$ discrepant from the theoretical expectation.

This discrepancy can be taken as evidence of a peculiar dynamical history of NGC 3201 or of some drawbacks due to the simplified framework adopted by Claydon et al. (2017) for the potential escaper calculation, which includes many uncertain ingredients, such as the initial condition of the GC, its orbit, and the Galactic potential. For example, if the cluster formed in a dwarf galaxy that later accreted onto the MW, it could have experienced a different tidal field than the one inferred by the current orbital properties. Therefore, the calculation of potential escapers presented in Claydon et al. (2017) would not be valid. Interestingly, an accreted origin of the cluster is also suggested by its current retrograde orbit (in analogy to ω Cen, suspected to be the stripped nucleus of an accreted dwarf galaxy; e.g., Freeman & Bland-Hawthorn 2002; Ibata et al. 2019). A similar scenario was recently suggested to interpret the morphology of the highly retrograde GD1 stellar stream, which is consistent with its progenitor having formed within a dark matter subhalo, later accreted onto the MW (Malhan et al. 2019a, 2019b).

As an alternative, the presence of a dark matter halo embedding the cluster, as a relic of its formation environment at redshift $z > 3$ (e.g., Peebles 1984; Ricotti et al. 2016), could naturally explain the flattening of the velocity dispersion. Interestingly, Peñarrubia et al. (2017) showed that the presence of a dark matter mini-halo can produce a gravitationally bound stellar envelope around a GC and a flattening of the velocity dispersion in the outskirts.

Finally, outside the Newtonian context, alternative theories of gravity such as MOND (e.g., Famaey & McGaugh 2012) could be invoked to explain our observations. The typical acceleration in the outskirts of the cluster is of the order of $\sim 3\,\sigma^2/R \approx 0.05 - 0.1\,a_0$, placing it in the MOND regime ($a_0 \sim 1.2 \times 10^{-10}\,\mathrm{m\,s^{-2}}$, characteristic scale of MOND). MOND would predict a velocity dispersion in the outskirts of the order of $\sigma^4 \approx G\,a_0\,M/\alpha^2$, with α the slope of the outer GC density profile. Given a value of $\alpha \approx -3.5$,[3] the predicted velocity dispersion would be $\approx$4–5 $\mathrm{km\,s^{-1}}$, remarkably similar to our observations. However, notice that the acceleration of the external field at the position of the cluster is of the order $\sim a_0$, larger than the typical acceleration of the GC itself. This external acceleration remains larger than the internal one even at apocenter. This implies that no flattening would be expected in MOND because of the external field effect (e.g., Haghi et al. 2011; Derakhshani 2014; Thomas et al. 2018), apart from possible effects due to the varying tidal field along the highly eccentric orbit of the GC.

5. Conclusions

In this Letter, we presented the first kinematic analysis of the GC NGC 3201, from the half-light radius to the outer regions beyond the Jacobi radius. We applied a strict selection to the *Gaia* DR2 data in order to exclude non-member contamination and retain only high-precision astrometric measurements. Our sample reveals the presence of extended stellar structure beyond the nominal tidal radius. This tidal tail structure is aligned along the southeast/northwest direction and extends to $\lesssim 2\,r_j$ ($\lesssim$100 pc).

Thanks to the 2D kinematics, we measured an anisotropic distribution in velocity space, characterized by radial anisotropy in the intermediate regions and a hint of isotropy in the outer parts. These signatures are consistent with the combined effects of internal relaxation processes and ongoing action of the MW tidal field. Moreover, the velocity maps show an excess of tangential velocity dispersion around the lobes formed by the tidal tails, indicating that stars on radial orbits preferentially escape around the Lagrangian points. A comparison with a GC *N*-body simulation with tidal tails displays qualitatively similar features for the anisotropy configuration.

Our analysis reveals flattened velocity dispersion profiles starting from the tidal radius ($\approx$40 pc) until beyond the Jacobi radius, settling around values of $\sim$2.5–4 $\mathrm{km\,s^{-1}}$, with an average velocity dispersion along the two components of $3.5 \pm 0.9\,\mathrm{km\,s^{-1}}$ at the Jacobi radius. This is in tension with what expected from the presence of potential escaper stars (Claydon et al. 2017) at a $\sim 3\sigma$ confidence level. However, note that we cannot exclude that small-scale systematics in the *Gaia*

[3] Calculated from the density profile of de Boer et al. (2019).

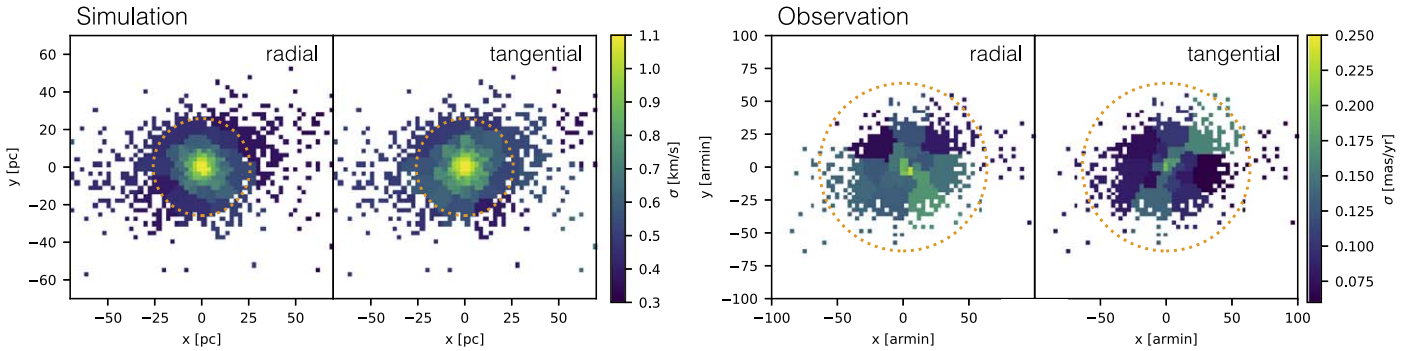

Figure 4. Comparison between velocity dispersion maps of the simulation (left panels) and the observation (right panels). A higher tangential velocity dispersion is observed along the northwest/southeast direction, in correspondence with the tidal tail overdensities. This feature can be explained by stars in radial orbits preferentially escaping the clusters to form the tidal tails, leaving an overabundance of stars in tangential orbits in proximity 0f the Lagrangian points. The dashed lines represent the Jacobi radii.

DR2 catalog could still produce an inflation of the velocity dispersion profiles of the order of <1 km s^{-1}. We propose that the observed discrepancy is due to a peculiar dynamical history of NGC 3201, which could have formed in a dwarf galaxy later accreted onto the MW, as also suggested by its retrograde and eccentric orbit. Similarly, the presence of a dark matter halo around the cluster could naturally produce flattened velocity dispersion profiles. This would favor the idea that GCs primordially formed in a dark matter mini-halo. Whether an alternative such as modified Newtonian dynamics could account for the observed discrepancy—despite that the external gravitational field dominates over the internal one—remains to be studied in detail in further works.

Our work shows that GC outskirts are the fundamental environment to unveil the formation properties of GCs, and possibly detect the presence of dark matter and deviations from standard Newtonian dynamics. The extension of our analysis to more GCs, together with the augmented precision of future *Gaia* data releases, the inclusion of line-of-sight data from future large surveys (e.g., WEAVE), and the comparison with tailored *N*-body simulations will allow us to address these problems in greater detail.

We thank the referee for the useful comments and suggestions. P.B. thanks Alice Zocchi, Anna Lisa Varri, and Lorenzo Posti for several stimulating discussions. R.I. and B.F. acknowledge funding from the Agence Nationale de la Recherche (ANR project ANR-18-CE31-0006) and from the European Research Council (ERC) under the European Unions Horizon 2020 research and innovation programme (grant agreement No. 834148). This work has made use of data from the European Space Agency (ESA) mission *Gaia* (https://www.cosmos.esa.int/gaia), processed by the *Gaia* Data Processing and Analysis Consortium (DPAC, https://www.cosmos.esa.int/web/gaia/dpac/consortium). Funding for the DPAC has been provided by national institutions, in particular the institutions participating in the *Gaia* Multilateral Agreement. This work made use of the PyGaia package provided by the *Gaia* Project Scientist Support Team and the *Gaia* Data Processing and Analysis Consortium (https://github.com/agabrown/PyGaia).

ORCID iDs

P. Bianchini https://orcid.org/0000-0002-0358-4502
R. Ibata https://orcid.org/0000-0002-3292-9709
B. Famaey https://orcid.org/0000-0003-3180-9825

References

Anguiano, B., De Silva, G. M., Freeman, K., et al. 2016, MNRAS, 457, 2078
Balbinot, E., & Gieles, M. 2018, MNRAS, 474, 2479
Baumgardt, H., & Hilker, M. 2018, MNRAS, 478, 1520
Baumgardt, H., & Makino, J. 2003, MNRAS, 340, 227
Bellazzini, M., Mucciarelli, A., Sollima, A., et al. 2015, MNRAS, 446, 3130
Bianchini, P., Sills, A., & Miholics, M. 2017, MNRAS, 471, 1181
Bianchini, P., van de Ven, G., Norris, M. A., Schinnerer, E., & Varri, A. L. 2016, MNRAS, 458, 3644
Bianchini, P., van der Marel, R. P., del Pino, A., et al. 2018a, MNRAS, 481, 2125
Bianchini, P., Webb, J. J., Sills, A., & Vesperini, E. 2018b, MNRAS, 475, L96
Cappellari, M., & Copin, Y. 2003, MNRAS, 342, 345
Carballo-Bello, J. A. 2019, MNRAS, 486, 1667
Chun, S.-H., Kim, J.-W., Sohn, S. T., et al. 2010, AJ, 139, 606
Claydon, I., Gieles, M., & Zocchi, A. 2017, MNRAS, 466, 3937
Da Costa, G. S. 2012, ApJ, 751, 6
Daniel, K. J., Heggie, D. C., & Varri, A. L. 2017, MNRAS, 468, 1453
de Boer, T. J. L., Gieles, M., Balbinot, E., et al. 2019, MNRAS, 485, 4906
Derakhshani, K. 2014, ApJ, 783, 48
Drukier, G. A., Slavin, S. D., Cohn, H. N., et al. 1998, AJ, 115, 708
Famaey, B., & McGaugh, S. S. 2012, LRR, 15, 10
Foreman-Mackey, D., Hogg, D. W., Lang, D., & Goodman, J. 2013, PASP, 125, 306
Freeman, K., & Bland-Hawthorn, J. 2002, ARA&A, 40, 487
Fukushige, T., & Heggie, D. C. 2000, MNRAS, 318, 753
Gaia Collaboration, Brown, A. G. A., Vallenari, A., et al. 2018a, A&A, 616, A1
Gaia Collaboration, Helmi, A., van Leeuwen, F., et al. 2018b, A&A, 616, A12
Grillmair, C. J., Freeman, K. C., Irwin, M., & Quinn, P. J. 1995, AJ, 109, 2553
Haghi, H., Baumgardt, H., & Kroupa, P. 2011, A&A, 527, A33
Harris, W. E. 1996, AJ, 112, 1487
Hernandez, X., Jiménez, M. A., & Allen, C. 2013, MNRAS, 428, 3196
Ibata, R., Nipoti, C., Sollima, A., et al. 2013, MNRAS, 428, 3648
Ibata, R. A., Bellazzini, M., Malhan, K., Martin, N., & Bianchini, P. 2019, NatAs, 3, 667
Jindal, A., Webb, J. J., & Bovy, J. 2019, MNRAS, 487, 3693
Kunder, A., Bono, G., Piffl, T., et al. 2014, A&A, 572, A30
Kundu, R., Minniti, D., & Singh, H. P. 2019, MNRAS, 483, 1737
Küpper, A. H. W., Kroupa, P., Baumgardt, H., & Heggie, D. C. 2010, MNRAS, 407, 2241
Kuzma, P. B., Da Costa, G. S., & Mackey, A. D. 2018, MNRAS, 473, 2881
Lane, R. R., Kiss, L. L., Lewis, G. F., et al. 2010, MNRAS, 406, 2732
Leaman, R., VandenBerg, D. A., & Mendel, J. T. 2013, MNRAS, 436, 122
Leon, S., Meylan, G., & Combes, F. 2000, A&A, 359, 907
Lindegren, L., Hernández, J., Bombrun, A., et al. 2018, A&A, 616, A2
Malhan, K., & Ibata, R. A. 2018, MNRAS, 477, 4063
Malhan, K., Ibata, R. A., Carlberg, R. G., et al. 2019a, ApJL, 886, L7
Malhan, K., Ibata, R. A., Carlberg, R. G., Valluri, M., & Freese, K. 2019b, ApJ, 881, 106
Marigo, P., Girardi, L., Bressan, A., et al. 2017, ApJ, 835, 77
Massari, D., Koppelman, H. H., & Helmi, A. 2019, A&A, 630, L4

McLaughlin, D. E., & van der Marel, R. P. 2005, ApJS, 161, 304
Miholics, M., Webb, J. J., & Sills, A. 2016, MNRAS, 456, 240
Peebles, P. J. E. 1984, ApJ, 277, 470
Peñarrubia, J., Varri, A. L., Breen, P. G., Ferguson, A. M. N., & Sánchez-Janssen, R. 2017, MNRAS, 471, L31
Renaud, F., & Gieles, M. 2015, MNRAS, 448, 3416
Ricotti, M., Parry, O. H., & Gnedin, N. Y. 2016, ApJ, 831, 204
Scarpa, R., Marconi, G., Gilmozzi, R., & Carraro, G. 2007, A&A, 462, L9
Sollima, A., Baumgardt, H., & Hilker, M. 2019, MNRAS, 485, 1460
Sollima, A., Baumgardt, H., Zocchi, A., et al. 2015, MNRAS, 451, 2185
Thomas, G. F., Famaey, B., Ibata, R., et al. 2018, A&A, 609, A44
Tiongco, M. A., Vesperini, E., & Varri, A. L. 2016, MNRAS, 455, 3693
Trenti, M., & van der Marel, R. 2013, MNRAS, 435, 3272
van de Ven, G., van den Bosch, R. C. E., Verolme, E. K., & de Zeeuw, P. T. 2006, A&A, 445, 513
Vasiliev, E. 2019, MNRAS, 489, 623
Zocchi, A., Bertin, G., & Varri, A. L. 2012, A&A, 539, A65
Zocchi, A., Gieles, M., Hénault-Brunet, V., & Varri, A. L. 2016, MNRAS, 462, 696